Full-duplex Airborne Ultrasonic Data Communication Using a Pilot-Aided QAM-OFDM Modulation Scheme

Wentao Jiang, *Student Member, IEEE,* and William M. D. Wright, *Senior Member, IEEE*

***Abstract*—Orthogonal frequency division multiplexing (OFDM) has been extensively used in a variety of broadband digital wireless communications applications because of its high bandwidth utilization efficiency and effective immunity to multipath distortion. This work has investigated quadrature amplitude modulation (QAM) and OFDM methods in air-coupled ultrasonic communication, using broadband capacitive ultrasonic transducers with high-k dielectric layers. OFDM phase noise was discussed and corrected using a pilot-aided estimation algorithm. The overall system data rate achieved was up to 400 kb/s with a spectral efficiency of 2 b/s/Hz. An ultrasonic propagation model for signal prediction considered atmospheric absorption of sound in air, beam divergence and transducer frequency response. The simulations were compared with experimental results, and good agreement was found between the two. Two-way communication through air was also implemented successfully by applying 3-way handshaking initialisation and an adaptive modulation scheme with variable data rates depending on the transmission distance, estimated using received signal strength indication (RSSI) measurement. It was shown that the error-free transmission range could be extended up to 2.5 m using different system transfer rates from 400 kb/s down to 100 kb/s. In full-deplex transmission mode, the overall error-free system data rate achieved was 0.8 Mb/s up to 1.5 m.**

Index Terms*— *Airborne ultrasonic communication, capacitive ultrasonic transducer, full-duplex, pilot-aided OFDM system.

I. Introduction

THERE has been recent interest in the use of airborne ultrasound for digital communications [1] due to its potential advantages over radio frequency (RF) communications. The radio spectrum is scarce and much of it is strictly regulated to control the performance of and prevent interference from different communication systems. Ultrasonic data transmission can be implemented by simple and inexpensive means at unregulated frequency bands, and in an interference-free manner in circumstances where radio emission is restricted. Compared to radio signals, ultrasonic signals are very difficult to intercept as ultrasonic waves do not easily penetrate through solid materials and do not travel long distances in air [2], [3] . This high security feature prevents airborne ultrasonic systems from malicious intervention such as eavesdropping and jamming attacks [1], [4]. In addition, ultrasonic based indoor positioning systems are becoming an increasingly popular solution as signal parameters such as time-of-flight can be measured more accurately owing to the slow propagation speed of ultrasound in air compared with radio waves [5], [6], [7].

Previous studies have looked at ultrasonic data transmission with practical hardware implementations. A hands-free telephone has been designed for transmitting digitized voice data by ultrasonic means through an air interface [8]. An indoor positioning system used in hospitals was developed based on frequency shift keying (FSK) modulated ultrasonic signals at 40 kHz [9]. The achieved transmission range in this work was up to 20 m, with a data transfer rate of 100 b/s. This work addressed some of the major challenges in air-coupled ultrasonic communications, including Doppler shift and reverberation, for robust and practical use. Other work also implemented an indoor location system, using broadband ultrasonic transmitter and receiver units [6]. This broadband system allowed the use of spread spectrum, multiple access techniques in its ranging signals and improved the overall data rate to 20 kb/s compared with narrowband ultrasonic location systems. Later works investigated different telecommunication modulation methods based on on-off keying (OOK), binary frequency-shift keying (BFSK), binary phase-shift keying (BPSK) and quadrature phase-shift keying (QPSK) for air-coupled ultrasonic data communication [4], [10]. The proposed solutions achieved data rates of up to 200 kb/s over a few metres using a pair of custom-made transducers. Previous studies by the authors have implemented multichannel amplitude-shift keying (ASK) modulation using both narrowband and broadband electrostatic transducers to improve bandwidth utilization efficiency [11], [12]. To further increase the spectral efficiency, OOK modulated orthogonal multichannel transmission was also presented by the authors, achieving a utilization rate of 1 b/s/Hz [13].

However, there are more advanced multichannel modulation formats available for airborne ultrasonic communication. Quadrature amplitude modulation (QAM) enables transmission of multiple bits per symbol, thus obtaining better levels of spectral efficiency than other forms of modulation [14]. QAM is usually combined with orthogonal frequency division multiplexing (OFDM) techniques to maximise the system throughput. Previous work in through-metal ultrasonic communication has successfully implemented OFDM using QAM achieving a raw throughput rate of up to 15 Mb/s and at a spectral efficiency of 3 b/s/Hz [15]. However, QAM-OFDM has not yet been applied to airborne systems. This work investigates the performance of QAM-OFDM scheme for two-way ultrasonic communications in air with the aim of maximising the data rate. Section II provides details of the implementation process

This work was supported by Science Foundation Ireland (SFI) Research Frontiers Programme grant number 11/RFP.1/ECE/3119.

of OFDM regarding modulation, transmission and demodulation techniques. The OFDM phase noise effects and the phase-amplitude correction mechanism are both explained in Section III. This is followed by the apparatus and experimental set-up of the work and experimental results in Sections IV and V, respectively. In Section VI, a two-way transmission with variable system transfer rates is presented. Section VII gives the conclusions of the work.

II. OFDM SYSTEM MODEL

A. OFDM modulation

To obtain maximum throughput, traditional multicarrier modulation schemes use a relatively smaller symbol duration. The system then becomes more susceptible to loss of information from impulse noise, multipath distortion and other impairments. In addition, a narrow frequency guard band between adjacent channels is unused to minimise the interference between modulated signals, but this lowers the overall bandwidth efficiency. OFDM is a special form of multicarrier transmission using a relatively longer symbol time, and with all the subcarriers orthogonal to each other, meaning that cross-talk between the subchannels is eliminated and guard bands are not required. The use of orthogonal subcarriers allows subcarrier spectra to overlap, thus significantly increasing the spectral efficiency. The orthogonality requires that the subcarrier spacing in frequency is [16]

$$f_d = k/T \tag{1}$$

in Hertz, where T is the symbol time in seconds, and k is a positive integer. For minimum overall signal bandwidth, k is usually set to 1. Base-band OFDM signals can be written mathematically as the sum of N modulated carriers

$$s(t) = \sum_{k=0}^{N-1} s_k e^{j2\pi k f_d t}. \tag{2}$$

Here s_k represents the OFDM symbol. Each transmitted symbol s_k takes on one of M possible signal states, and can be denoted as $s_k \in [s^{(1)}, s^{(2)}, ..., s^{(M)}]$. For example, $M = 2$, if BPSK modulation is used. In practice, both modulation and multiplexing are achieved digitally using an inverse fast Fourier transform (IFFT). As a result, the required orthogonal signals can be generated precisely and in a very computationally efficient way. Taking N sampling points of the signal $s(t)$ which is of symbol duration T, discrete values may be obtained at $t_n = n \cdot T/N$, $n = 0, 1, ..., N-1$, where T/N is the sample interval. This yields

$$s(n) = s(t_n) = \sum_{k=0}^{N-1} s_k e^{j\frac{2\pi}{N} k f_d n T}. \tag{3}$$

As $f_d = 1/T$, $s(n)$ may then be expressed by

$$\begin{aligned} s(n) &= \sum_{k=0}^{N-1} s_k e^{j\frac{2\pi}{N} kn} \\ &= N \times IFFT[s_k], \qquad n = 0, 1, ..., N-1. \end{aligned} \tag{4}$$

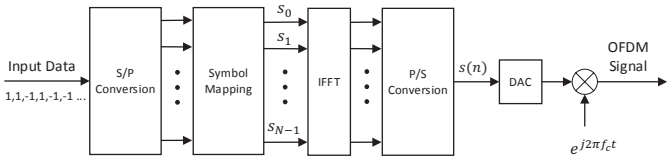

Fig. 1: Schematic diagram of an OFDM modulator.

Therefore, the OFDM signal $s(n)$ can be calculated very efficiently by applying IFFT to the set of OFDM symbols s_k.

A typical OFDM modulator [17] is described in Fig. 1. In the digital domain, a series of input binary data is collected and converted to parallel combinations before mapping to corresponding constellation points on a constellation diagram, which is the two-dimensional plot of the signal states from a sequence of symbols. In this paper, binary signals are modulated using a 4-QAM scheme. At this point, the OFDM symbols, s_k, are presented as random-value complex numbers from the 4-QAM constellation $\frac{\sqrt{2}}{2} \cdot \{1+j, 1-j, -1+j, -1-j\}$. An IFFT operation is then performed on the parallel complex data, and a parallel-to-serial converter is then applied to produce the base-band OFDM signal, $s(n)$, which contains the original band of frequencies before it is modulated for transmission at a higher frequency. After that, a digital-to-analogue converter (DAC) is used to transform time-domain digital data to time-domain analogue data before up-converting the signal to the transmission frequency, f_c. At this point in time, the input data are OFDM modulated and ready to be transmitted.

B. OFDM transmission

The structure of the transmitted signal sequence is presented in Fig. 2. The sequence contains two major parts: preamble and data. In the preamble section, a linear frequency modulation (LFM) signal [18] is transmitted at the start of the sequence for wireless synchronisation. The LFM signal is described by the following equation

$$s(t) = Acos[2\pi t(f_0 + \frac{k}{2}t) + \phi]. \tag{5}$$

Here, f_0 is the starting frequency and k is the rate of frequency change. The frequency of the LFM signal is modulated in a linear manner with time from a low frequency to a high frequency. By performing correlation of a known LFM signal and the received signal using a matched-filter at the receiver, the maximum energy of the matched-filter output indicates the start of the arriving data sequence as shown in Fig. 2. The main advantage of using a LFM signal is that it provides precise timing resolution for frame synchronisation as the matched-filter is the optimal linear filter that maximises the signal-to-noise ratio (SNR) in the presence of additive stochastic noise [19], [20]. The LFM preamble is followed by the OFDM pilot signal. This is used to correct the OFDM phase noise, and will be explained in detail in section IV. Note that zero padding is inserted between each type of signal packet to help distinguish one from another.

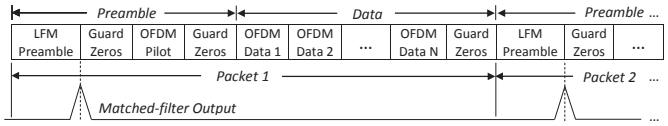

Fig. 2: Data structure of transmitted sequence.

When modelling ultrasonic signal transmissions in air, three filters to compensate for absorption of sound in air, beam divergence and transducer frequency response should be included. The atmospheric absorption factor α is measured in dB/m and can be expressed as [21]

$$\alpha = f^2 \left[1.59 \times 10^{-10} \left(\frac{P_0}{P}\right) \left(\frac{T}{T_0}\right)^{\frac{1}{2}} + 0.111 \left(\frac{T}{T_0}\right)^{-\frac{5}{2}} \frac{e^{\frac{-2239.1}{T}}}{f_{r,O} + \frac{f^2}{f_{r,O}}} + 0.929 \frac{e^{\frac{-3352}{T}}}{f_{r,N} + \frac{f^2}{f_{r,N}}} \right]. \quad (6)$$

Here, P_0 is the reference pressure (101.325 kPa) and P is the measured pressure. T_0 and T are the reference temperature (293.15 K) and the measured temperature (in K), respectively. f is the frequency of the ultrasonic wave. The terms $f_{r,O}$ and $f_{r,N}$ are, respectively, the frequencies of maximum absorption for oxygen and nitrogen in Hertz. Due to diffraction effects, the ultrasound beam diverges from the transmitter aperture. Different amounts of the transmitted energy will be intercepted by the receiver depending on the propagation range and the frequencies used. The beam spread angle γ for a circular transducer is approximated by [22]

$$sin\ \gamma = 1.22\lambda/D \quad (7)$$

where λ is the ultrasonic wavelength and D is the aperture of the ultrasonic transducer. The received signal energy can then be calculated in terms of the ratio of the transducer radius and the beam spread radius at a particular range. The received signal is also shaped by both the transmitter and receiver transducer responses at different subcarrier frequencies. To simplify the simulation, an impulse signal was sent from the transmitter to the receiver transducer with minimum separation, the transducer frequency response was then calculated based on the impulse signal captured by the receiver. The received signal over different transmission ranges can then be simulated and predicted by implementing the above three filters.

C. OFDM demodulation

The demodulation for an OFDM signal is essentially the reverse process of the modulation as illustrated in Fig. 3. After receiving the OFDM signal, the receiver down-converts it and transforms it to the digital domain using an analogue-to-digital converter (ADC). After ADC conversion, the time-domain base-band OFDM signal, $r(n)$, is demodulated and converted to the frequency domain by executing a fast Fourier transform (FFT), avoiding the need for complex subchannel filters. A phase offset recovery scheme together with channel

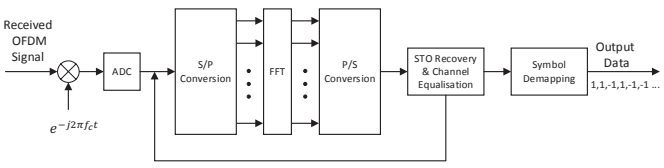

Fig. 3: Schematic diagram of an OFDM demodulator.

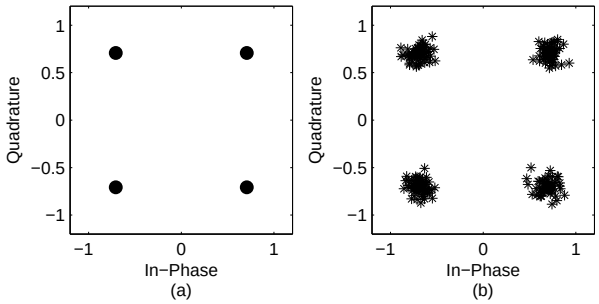

Fig. 4: Simulated 4-QAM OFDM signal constellation diagrams: (a) ideal and (b) AWGN added for an SNR of 5 dB.

equalisation is performed with the aid of the OFDM pilot signal. How these schemes work will be explained in section IV. After that, corrected OFDM symbols are de-mapped according to the transmission constellation pattern. Fig. 4 (a) shows an ideal received 4QAM-OFDM signal constellation plot with all constellations exactly on the original points. If additive white Gaussian noise (AWGN) is applied to the transmitted signal, the demodulated constellations are scattered around the original points as illustrated in Fig. 4 (b). As can be seen, the amplitude and phase presentation of the subcarrier signals are changed after introducing the noise, but all received constellations are well separated and all the transmitted bits can still be correctly decoded.

III. Phase noise effects and correction

Generally, it is critical to perform an accurate time synchronisation to allow a receiver to recover an OFDM signal. An N-point FFT at the receiver processes data in blocks of N samples at a time. Ideally, the N samples taken in by the FFT will correspond to the N samples of a single transmitted OFDM symbol. As described in Fig. 2, a known LFM preamble is located at the start of the data sequence for frame synchronisation. By processing the correlation operation, this aids the receiver to detect the OFDM symbol boundary. However, inaccuracy may still remain, and this is known as symbol timing offset (STO). The result is that the N samples sent to the FFT do not line up with the corresponding OFDM symbol. Thus, this offset can also be viewed as a shift of the FFT window. Assuming the symbol timing offset is δ samples, the received signal, $r(n)$, will then be a shifted version of $s(n)$ in (4), expressed as:

$$\begin{aligned} r(n) &= s(n+\delta) \\ &= \sum_{k=0}^{N-1} s_k e^{j\frac{2\pi}{N}k(n+\delta)}, \qquad n = 0, 1, ..., N-1. \end{aligned} \quad (8)$$

Applying an FFT to both sides of (8) allows the recovered

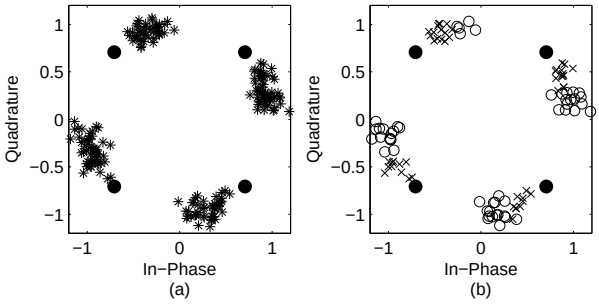

Fig. 5: Effect of STO on received constellation: (a) Phase shift with 2 samples of symbol offset, SNR=5 dB, (b) Phase shift with 2 samples symbol offset showing only the lowest and the highest frequency constellation points: low frequencies (×) and high frequencies (○).

complex number sequence for each OFDM symbol to be derived as:

$$\begin{aligned} y_k &= \sum_{n=0}^{N-1} \left\{ \sum_{l=0}^{N-1} s_k e^{j\frac{2\pi}{N}k(n+\delta)} \right\} \cdot e^{-j\frac{2\pi}{N}kn} \\ &= s_k \cdot e^{j\frac{2\pi}{N}k\delta}, \qquad k = 0, 1, ..., N-1. \end{aligned} \tag{9}$$

As (9) shows, an STO of δ samples in the time domain incurs a phase offset of $\frac{2\pi}{N}k\delta$ in the frequency domain, which is proportional to the subcarrier index k, as well as the STO. This means that the STO error does not destroy the orthogonality of the subcarriers, and the effect of the timing error is a phase rotation which linearly changes with carrier index. A simulated example of an OFDM signal shifted by 2 samples is shown in Fig. 5. As can be seen in Fig. 5 (b), constellations of subcarriers corresponding to high frequencies experience a larger rotation than low frequency ones.

STO can be corrected by applying the maximum likelihood (ML) approach [20] to the data-aided phase recovery scheme. Mathematically, it is to minimise the difference between the received pilot signal and the signal of interest:

$$\begin{aligned} \hat{\delta} &= \arg\min_{\delta} \left\{ \sum_{n=0}^{N-1} \left[s(n) - s(n+\delta) \right]^2 \right\} \\ &= \arg\min_{\delta} \left\{ \sum_{n=0}^{N-1} s^2(n) - 2\sum_{n=0}^{N-1} s(n)s(n+\delta) + \sum_{n=0}^{N-1} s^2(n+\delta) \right\}. \end{aligned} \tag{10}$$

Note that the first term of the expansion in (10) does not depend on the unknown parameter δ, thus it will not affect the optimisation process. In the second term, the parameter is present, however, the sum is the energy of the signal, and when δ changes, the energy is still the same. Thus the second term of the expansion does not depend on δ either, and it can be removed from the optimisation process. Therefore, the maximisation becomes:

$$\hat{\delta} = \arg\max_{\delta} \left\{ \sum_{n=0}^{N-1} s(n)s(n+\delta) \right\}. \tag{11}$$

The sum in (11) is actually the time-correlation between the received signal and the signal of interest. Therefore, in this particular case, the ML approach is equivalent to the maximisation of the correlation. In practice, this optimisation process is performed using functional blocks as depicted in Fig. 6. An ADC converter samples a received OFDM signal. An FFT window is controlled by an FFT window controller to recover an FFT window position. A phase difference calculator calculates a phase difference between the original pilot and the received pilot signal extracted by a pilot extractor. An FFT window offset detector then detects the position of the FFT window by the phase difference output from the phase difference calculator. After that, the FFT window controller controls the position of the FFT window by the FFT window offset. Apart from the STO recovery, channel equalisation is also carried out based on the received pilot signal to equalise the amplitudes of the signals at different subcarriers as the air channel has a non-flat frequency response.

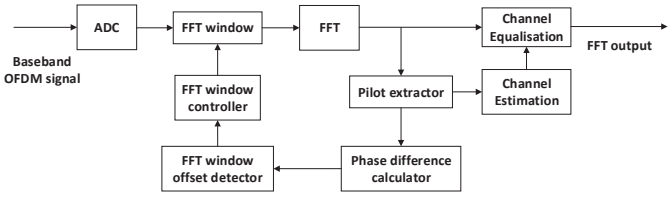

Fig. 6: Structure of STO synchronisation.

IV. Apparatus and experiment set-up

Fig. 7 illustrates the experimental arrangement for a two-way, full-duplex OFDM transmission using two pairs of prototype airborne capacitive ultrasonic transducers with high-k coated backplates [23]. The data signal was modulated by MATLAB running on a PC before sending it to a TTi TGA 12102 arbitrary waveform generator using a GPIB interface. The signal was then amplified using a Falco WMA-200 high voltage amplifier, and combined with a superimposed +200 V DC bias voltage generated by a Delta Elektronika SM3004-D power supply. The transmitter had a HfO_2 high-k layer with a thickness of 800 nm uniformly distributed across the pitted backplate, and covered by a 5 μm metallized PET membrane, assembled into a screened casing with a 10 mm diameter aperture. The receiver, manufactured in the same way as the transmitter, was connected to a Cooknell CA6/C charge amplifier powered by a Cooknell SU2/C power supply unit, and followed by a high performance PicoScope 6403A PC oscilloscope. After that, the captured signal was sent back to another PC via a USB interface for signal processing.

The overall system amplitude and phase response over an air channel at 0.5 m are illustrated in Fig. 8 (a) and (b) respectively. The received impulse was measured by sending a pulse signal generated by a Panametrics 500PR pulser from the transmitter to the receiver. As can be seen in Fig. 8 (a), the spectrum peaks at about 250 kHz, with a significant decline in response above 500 kHz. Fig. 8 (b) shows that the phase response of the channel is nearly linear at frequencies under 700 kHz. Note that the output signal amplitude was typically 175 V peak-to-peak after amplification. The recorded received signal amplitude was typically around 8 mV rms at 0.5 m, and

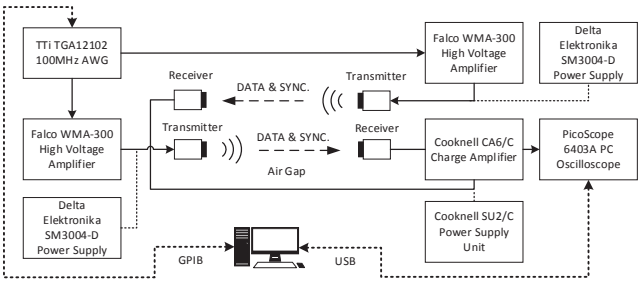

Fig. 7: Schematic diagram of the experimental set-up.

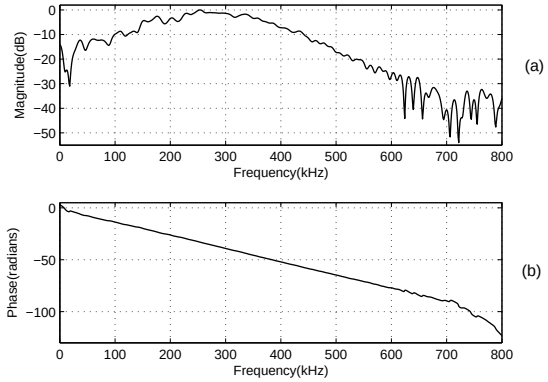

Fig. 8: System characteristics: (a) system response and (b) phase response.

the rms amplitude of the background noise was about 450 μV giving an SNR of 25 dB at this range.

V. Results and discussion

All experiments were carried out in an indoor laboratory with negligible air turbulence. Transmitter and receiver transducers were separated in a line-of-sight (LOS) manner, and the transmission bandwidth used was from 150 to 350 kHz. The system data rate achieved was 400 kb/s as the symbol duration was set at 1 ms. The measured sound pressure level (SPL) of a 10 kHz signal at 0.5 m was 64 dB. According to the system response in Fig. 8 (a), the estimated output level was 89 dB at the centre frequency of 250 kHz. The measured background noise level was similarly recorded as 39 dB at 250 kHz. Fig. 9 compares the transmitted signal, simulated received signal and actual received signal at transmission distances of 0.5 m and 1.6 m in both time domain and frequency domain. As can be seen, there is good agreement between the simulation predictions and actual experimental signals. In particular, at a short transmission range (0.5 m), it can be observed that the positive slope of the spectra outline from 150 to 350 kHz in Fig. 9 (d) and (f) indicate that low frequency channel signals suffer from more significant loss due to beam divergence. However, over longer ranges (1.6 m), atmospheric absorption contributes more attenuation to high frequency channel signals as the spectra outlines have a negative slope along the frequency axis as shown in Fig. 9 (h) and (j). Unlike single-carrier systems, OFDM schemes for high data rate applications are very sensitive to phase noise. As shown in Fig. 10, the constellations of the received signals before phase correction are completely corrupted as all the constellation points are spread across the quadrature boundary. In this case, the received signal could not be correctly decoded. After phase noise correction, the signal constellations are well presented in four constellation regions at both 0.5 m and 1.6 m ranges, as shown in Fig. 11 and Fig. 12 respectively. The actual received signal constellations in Fig. 11 (c) and Fig. 12 (c) are compared with the simulated constellations in Fig. 11 (a) and Fig. 12 (a). It can be seen that the theoretical predictions match the experimental signals well. The highest and the lowest 50 channel constellations are clustered into two groups with different amplitude levels due to both atmospheric attenuation and beam divergence. As can be seen from Fig. 11 (b) and (d), when the transmission range is short, low frequency constellations present lower amplitudes than high frequency ones. In Fig. 12 (b) and (d), as transmission range increases, the amplitudes of high frequency constellations start to decrease and become smaller than low frequency constellation amplitudes. To perform a better identification of symbols, channel equalisation was applied to provide tightly clustered constellation points. This can either be done with the aid of the pilot signal or using the simulation model. Fig. 13 (a) and (b) compares the outputs of the phase difference calculator when using the pilot signal and using the simulation model at transmission distances of 0.5 m and 1.6 m respectively. It shows an excellent agreement between the prediction of the simulation and the actual experimental phase difference calculated using the pilot signal. In Fig. 13 (a), when transmission distance is 0.5 m, the amplitude differences increase in both simulation and experiment as the subcarrier frequency increases. This trend confirms the results shown in both Fig. 9 and Fig. 11 at the same transmission distance. For the increased transmission distance (1.6 m), the opposite trend occurs, as shown in 13 (b) for both simulation experiment. It again demonstrates that the atmospheric absorption dominates the total attenuation with the increase of the subcarrier frequency. Fig. 14 (a) and (b) present the constellation diagrams after channel equalisation using theoretical prediction and the experimental pilot signal respectively at 1.6 m. As can be seen, constellations are clustered together in their individual regions in the same way as the constellation pattern shown in Fig. 4 (b). The equalisation compensates the amplitude difference between different subcarrier signals. This is also necessary for correct decoding of higher-order quadrature modulation schemes such as 16-QAM, 64-QAM and so on.

Transmission reliability was evaluated according to bit error rate (BER) tests at different ranges. Therefore, randomly generated 400-bit binary streams were modulated using the 4-QAM OFDM scheme and transmitted through the air channel. Received signals were decoded at an increasing range up to 2.5 m with an increment of 0.1 m. The process was repeated 10 times before averaging. Due to hardware limitations, only 90 OFDM data packets could be transmitted each time, which gave a total number of 360,000 bits being transmitted for the BER test at each range. Fig. 15 shows that the system started to have error decoding at 1.7 m and the number of incorrectly decoded bits increased with the transmission range, as expected. The BERs of different subcarriers at a transmission range of 2.5 m are shown in Fig. 16. As can

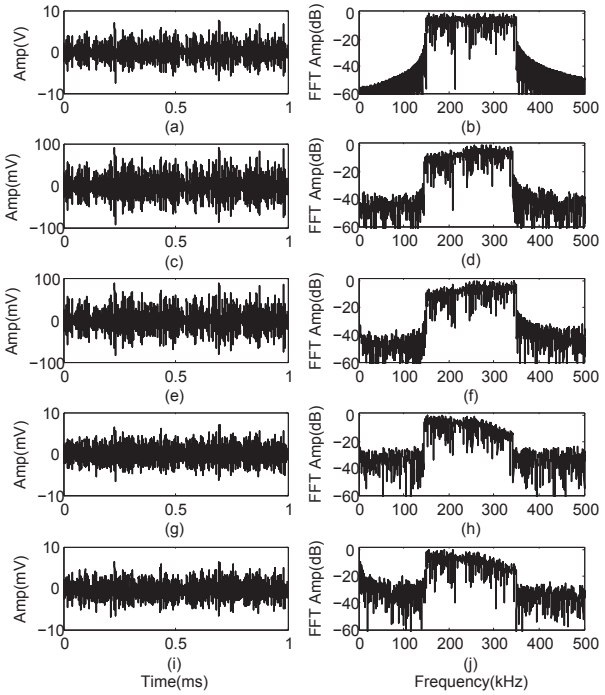

Fig. 9: Comparison of transmitted signal, simulated received signal and actual received signal over 0.5 m and 1.6 m: (a) time domain transmitted signal, (b) its spectra, (c) time domain simulated received signal at 0.5 m, (d) its spectra, (e) actual received signal in time domain at 0.5 m, (f) its spectra, (g) time domain simulated received signal at 1.6 m, (h) its spectra, (i) actual received signal in time domain at 1.6 m, (j) its spectra.

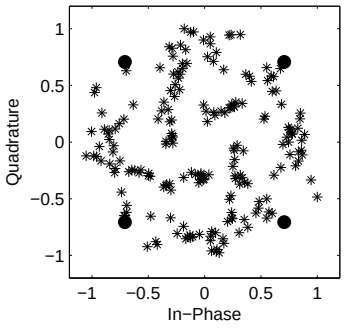

Fig. 10: Received signal constellation before STO recovery and equalisation.

be seen, high frequency subcarriers contributed most of the errors, and the number of errors increases with the increase of carrier frequency. It indicates that a slower data rate using low frequency subcarriers would possibly improve overall signal quality and extend the error-free transmission range. Details of error-free transmission ranges with various communication rates are shown in Table I. Error-free transmission range could be extended up to 2.5 m by gradually reducing the data transfer rate from 400 kb/s to 100 kb/s. It should be noted that low data-rate OFDM signal transmissions, over larger distances, may also be achieved by using narrow-band air-coupled piezoelectric ultrasonic transducers [24] where higher sensitivity and improved propagation efficiency may be obtained.

In a typical indoor office or laboratory environment, air movement introduced by ventilation fans or air conditioning,

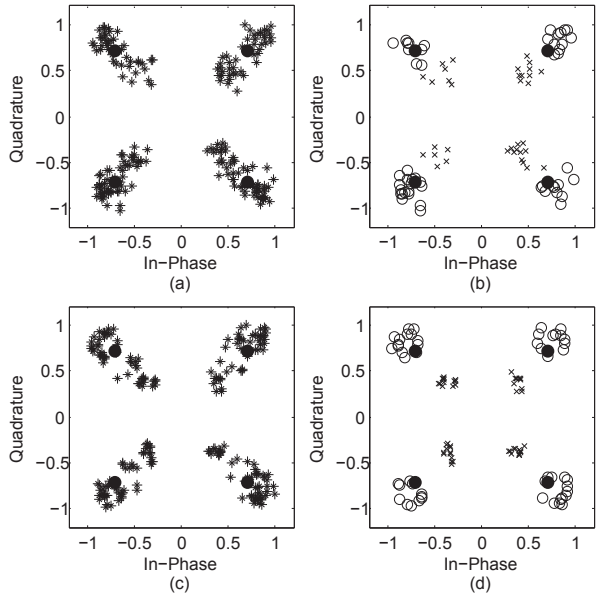

Fig. 11: Comparison of received signal constellation after phase correction in simulation at a transmission distance of 0.5 m: (a) signal constellations at all subcarrier channels, (b) received signal constellation showing only the lowest and the highest frequency constellation points: low frequencies (×) and high frequencies (○). Corresponding constellations of experimental signals (c) and (d) at a transmission distance of 0.5 m.

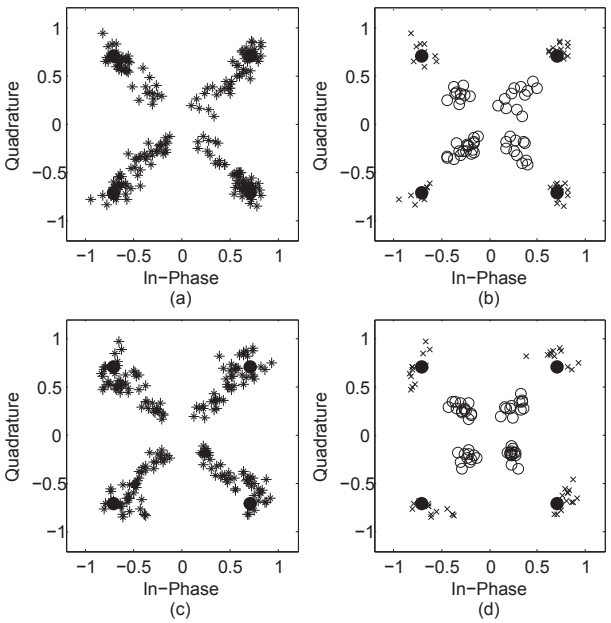

Fig. 12: Comparison of received signal constellation after phase correction in simulation at a transmission distance of 1.6 m: (a) signal constellations at all subcarrier channels, (b) received signal constellation showing only the lowest and the highest frequency constellation points: low frequencies (×) and high frequencies (○). Corresponding constellations of experimental signals (c) and (d) at a transmission distance of 1.6 m.

or relative motion between source and receiver, may produce Doppler shift which would affect the signal transmission. By placing a small axial flow fan at the receiver side and gradually increasing the rotation speed of the fan, it was found that error-free decoding was achieved when the speed of air flow was below 3.5 km/h (0.97 m/s, slow walking pace) in both

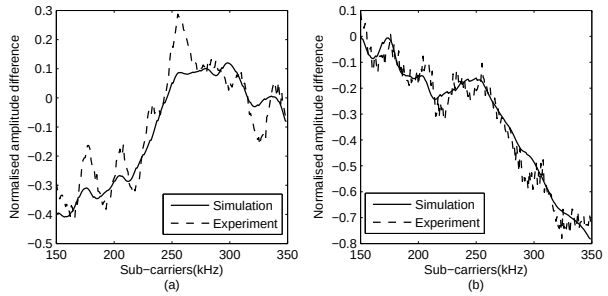

Fig. 13: Amplitude difference estimated by the experimental pilot signal and by the simulation model in transmission distances of (a) 0.5 m and (b) 1.6 m.

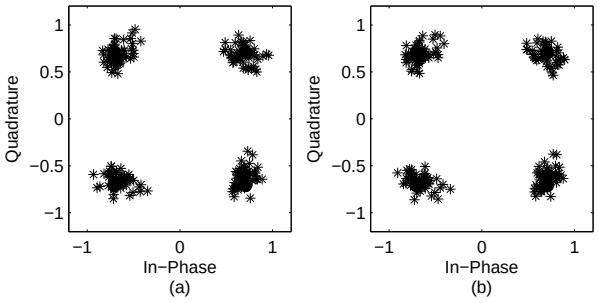

Fig. 14: (a) Received signal constellation after channel equalisation using the simulation model, and (b) received signal constellation after channel equalisation with the aid of the experimental pilot signal.

the axial and radial directions, with the transmitter separated from the receiver by 1 m. By observing the received time-domain signals, amplitude variations and jitter were found to be the dominant effects when the air flow was in the axial and radial directions, respectively. High-frequency channels were more prone to error as the number of incorrectly decoded bits increased with the subcarrier frequency. Since the system tolerance to axial air flow was up to 3.5 km/h, the system should still work properly if the maximum Doppler shift is under this level. Previous work by the authors [25] has studied air-coupled ultrasonic communication when the transducer centre normals are misaligned. It showed that a similar system can tolerate errors with a small amount of lateral displacement and oblique angles. Highly divergent or omnidirectional transducers would be required for better signal reception.

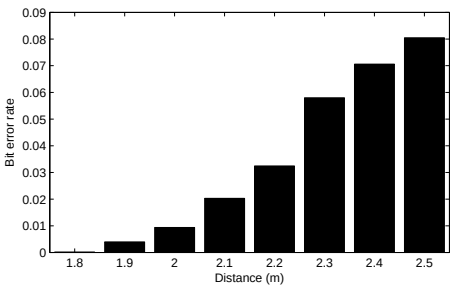

Fig. 15: BER result of 4QAM-OFDM modulation at different transmission ranges.

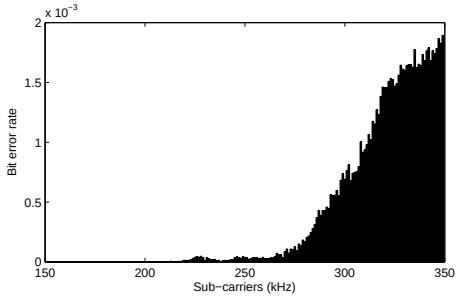

Fig. 16: BER result of different subcarriers at a transmission range of 2.5 m.

TABLE I: Error-free transmission ranges with various data rates up to 2.5 m

Sub-carriers (kHz)	Data rate (kb/s)	Error-free transmission range (m)
150 - 350	400	1.7
150 - 300	300	2
150 - 250	200	2.1
150 - 200	100	2.5

VI. Two-way data transmission

After demonstrating the feasibility of 4-QAM OFDM using airborne ultrasound, two pairs of capacitive high-k ultrasonic transducers were used to establish a two-way ultrasonic communication link. Before any data can be transmitted, a reliable connection must be obtained and acknowledged. Therefore, a 3-way handshaking technique was used to initialise the transmission. Fig. 17 illustrates a diagram of the 3-way handshake process. To establish the connection, host A sends a synchronization (SYNC.A) message containing randomly generated binary bits to host B. Then if host B receives the SYNC.A message, it extracts the bit information and sends back an acknowledge (ACK.B) message (equal to SYNC.A+1) followed by a new SYNC.B message generated by host B. Once host A receives the ACK-SYNC message, it checks the ACK.B message and sends back a new ACK.A message which is equal to SYNC.B+1. After host B detects the correct ACK.A message, the connection is then established. At this point, host B will send a test signal to host A. Here a received signal strength indication (RSSI) method is used as a distance measurement [26], [27]. Host A then calculates the rms value of the test signal and estimates the distance by applying the propagation model of ultrasonic signals in air described earlier in Section II-B. Afterwards, the corresponding modulation id based on the estimated distance is sent back to host B. Eventually, host B starts to send data modulated by the 4-QAM modulation scheme. Fig. 17 presents a half-duplex transmission, in practice, a full-duplex communication is usually required for a wireless system. Therefore, the full-duplex transmission with 400 kb/s data rate was evaluated and compared with the half-duplex transmission in terms of the BER at different ranges as shown in Fig. 18. As can be seen, full-duplex communication experienced a higher BER than that of half-duplex transmission at all ranges due to interference between the two signals propagating simultaneously across the air gap. The reliable error-free transmission range using full-duplex was also reduced to 1.5 m. Again, most of the BERs occurred at high frequency subcarriers. As both sides transmitted data

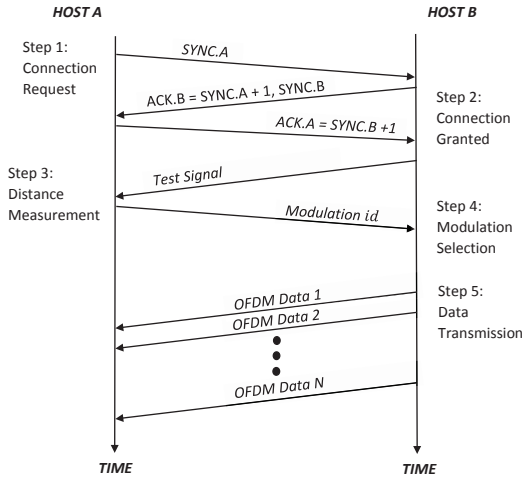

Fig. 17: 3-way hand shake and range-selected modulation mechanism.

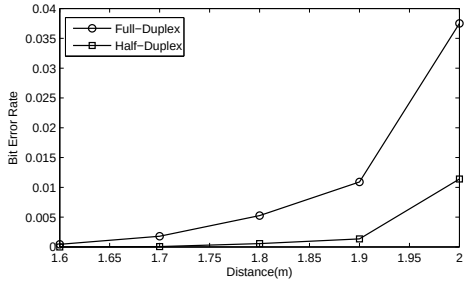

Fig. 18: Comparison of BERs for full-duplex and half-duplex transmission at different ranges.

using the same frequency band, the overall system transfer rate achieved was at 0.8 Mb/s in a full-duplex mode.

VII. Conclusions

This paper presented a successful implementation of a pilot-aided QAM-OFDM data communication in air using prototype capacitive ultrasonic transducers with a high-k dielectric coating. Phase noise due to STO was explained and corrected in advance of OFDM demodulation and demultiplexing by executing a pilot-aided estimation algorithm. The overall system data rate was 400 kb/s with a spectral efficiency of 2 b/s/Hz. Two-way communication with an adaptive transmission scheme was also introduced in the paper. The transmission was initialised using 3-way handshaking and propagation distance was estimated using RSSI measurement and a propagation model of the ultrasonic transmissions. Adaptive modulation methods were then applied according to the detected range. Error-free transmission was achieved at ranges up to 2.5 m with variable data rates from 400 kb/s down to 100 kb/s. In full-duplex transmission mode, it has been shown that the reliable overall system data rate achieved was 0.8 Mb/s up to 1.5 m. As the work in this paper was performed over relatively short distances and in a direct LOS manner, the study assumed no multipath reflections. In practice, non-LOS transmissions including diffraction and multiple reflections may occur and system robustness under movement needs to be considered. All these factors are currently under investigation.

References

[1] K. Nakamura, Ed., *Ultrasonic Transducers: Materials and Design for Sensors, Actuators and Medical Applications*. Woodhead Publishing Limited, 2012.

[2] R. Adler, P. Desmares, and J. Spracklen, "An ultrasonic remote control for home receivers," *IEEE Trans. Consum. Electron.*, vol. CE-28, no. 1, pp. 123–128, Feb 1982.

[3] D. Schindel and D. Hutchins, "Applications of micromachined capacitance transducers in air-coupled ultrasonics and nondestructive evaluation," *IEEE Trans. Ultrason., Ferroelect., Freq. Control*, vol. 42, no. 1, pp. 51–58, Jan 1995.

[4] C. Li, D. Hutchins, and R. Green, "Short-range ultrasonic communications in air using quadrature modulation," *IEEE Trans. Ultrason., Ferroelect., Freq. Control*, vol. 56, no. 10, pp. 2060–2072, 2009.

[5] S. Holm, "Airborne ultrasound data communications: the core of an indoor positioning system," in *Proc. IEEE Int. Ultrason. Symp. (IUS)*, vol. 3, Sept. 2005, pp. 1801–1804.

[6] M. Hazas and A. Hopper, "Broadband ultrasonic location systems for improved indoor positioning," *IEEE Trans. Mobile Comput.*, vol. 5, no. 5, pp. 536–547, May 2006.

[7] M. Saad, C. J. Bleakley, T. Ballal, and S. Dobson, "High-accuracy reference-free ultrasonic location estimation," *IEEE Trans. Instrum. Meas.*, vol. 61, no. 6, pp. 1561–1570, June 2012.

[8] L. Hofmann, "Transmission of data by ultrasound," U.S. Patent 6 950 681, Sep. 27, 2005.

[9] S. Holm, O. Hovind, S. Rostad, and R. Holm, "Indoors data communications using airborne ultrasound," in *Proc. IEEE Int. Acoust. Speech. Signal (ICASSP'05)*, vol. 3, Mar. 2005, pp. 957–960.

[10] C. Li, D. Hutchins, and R. Green, "Short-range ultrasonic digital communications in air," *IEEE Trans. Ultrason., Ferroelect., Freq. Control*, vol. 55, no. 4, pp. 908–918, 2008.

[11] W. Jiang and W. Wright, "Wireless communication using ultrasound in air with parallel OOK channels," in *Proc. 24th IET Irish Signals Syst. Conf. (ISSC'13)*, Jun. 2013, pp. 1–6.

[12] W. Jiang and W. M. D. Wright, "Multi-channel indoor wireless data communication using high-k capacitive ultrasonic transducers in air," in *Proc. IEEE Int. Ultrason. Symp. (IUS)*, Jul. 2013, pp. 1606–1609.

[13] W. Jiang and W. Wright, "Ultrasonic wireless communication in air using OFDM-OOK modulation," in *Proc. IEEE Int. Ultrason. Symp. (IUS)*, Sept. 2014, pp. 1025–1028.

[14] I. Glover and P. Grant, *Digital Communications*. Prentice Hall, 1998.

[15] K. Wanuga, M. Bielinski, R. Primerano, M. Kam, and K. Dandekar, "High-data-rate ultrasonic through-metal communication," *IEEE Trans. Ultrason., Ferroelect., Freq. Control*, vol. 59, no. 9, pp. 2051–2053, Sept. 2012.

[16] E. McCune, *Practical digital wireless signals*. Cambridge University Press, 2010.

[17] J. Bingham, "Multicarrier modulation for data transmission: an idea whose time has come," *IEEE Commun. Mag.*, vol. 28, no. 5, pp. 5–14, May 1990.

[18] M. Skolnik, *Introduction to Radar Systems*, ser. Electrical engineering series. McGraw Hill, 2001.

[19] P. Lazik and A. Rowe, "Indoor pseudo-ranging of mobile devices using ultrasonic chirps," in *Proc. 10th ACM Conf. Embedded Netw. Sensor Syst.*, Nov. 2012, pp. 99–112.

[20] J. Proakis and M. Salehi, *Digital Communications*. McGraw-Hill Higher Education, 2008.

[21] W. Mason and R. Thurston, Eds., *Physical acoustics: principles and methods*, ser. Physical Acoustics. Academic Press, 1984.

[22] J. Krautkrämer and H. Krautkrämer, *Ultrasonic testing of materials*. Springer-Verlag, 1990.

[23] S. G. McSweeney and W. M. D. Wright, "HfO_2 high-k dielectric layers in air-coupled capacitive ultrasonic transducers," in *Proc. IEEE Int. Ultrason. Symp. (IUS)*, Oct. 2011, pp. 864–867.

[24] W. A. Grandia and C. M. Fortunko, "NDE applications of air-coupled ultrasonic transducers," in *Proc. IEEE Int. Ultrason. Symp. (IUS)*, vol. 1, Nov. 1995, pp. 697–709.

[25] W. Jiang and W. Wright, "Multi-channel ultrasonic data communications in air using range-dependent modulation schemes," *IEEE Trans. Ultrason., Ferroelect., Freq. Control*, vol. PP, no. 99, pp. 1–1, 2015.

[26] S. Holm, "Ultrasound positioning based on time-of-flight and signal strength," in *Proc. Int. Conf. Indoor Position. Indoor Navigat. (IPIN)*, Nov. 2012, pp. 1–6.

[27] C. Medina, J. Segura, and S. Holm, "Feasibility of ultrasound positioning based on signal strength," in *Proc. Int. Conf. Indoor Position. Indoor Navigat. (IPIN)*, Nov. 2012, pp. 1–9.